Chapter 4

SIMULATION OF ISA CONCEPT

This chapter includes both published work from the following proceedings and new, unpublished sections:

J. Suh, S. P. Dassanayake, and S. Pellegrino, "In-Space Assembly of Large Mesh Reflectors," in *AIAA SCITECH 2025 Forum [Accepted]*, 2025.

J. Suh, S. P. Dassanayake, M. Thomson, and S. Pellegrino, "In-Space Assembly of Large Mesh Reflector Antennas," in *Aerospace Structures, Structural Dynamics, and Materials Conference, SSDM 2024 [Technical Presentation]*, 2024, p. 137 740.

4.1 Motivation

ISA poses significant challenges, particularly as the number of structural components increases and different assumptions about the assembly sequence come into play. As outlined in Section 1.4, a critical issue is ensuring that the assembly process proceeds smoothly, avoiding potential snags, jams, or misalignments that can occur when components interact unexpectedly. The complexity increases with larger structures, making it difficult to predict how different parts will behave during assembly. As the structure grows, the risk of interference between components rises, leading to potential delays or complications that may hinder the overall process.

Another challenge lies in the order of assembly, which directly affects both the ease of construction and the structural integrity of the final design. A poorly planned sequence can introduce unnecessary stresses or misalignments. This necessitates careful planning, with each step of the assembly process thoroughly considered to maintain stability and functionality as new components are integrated.

To manage these issues effectively, advanced numerical simulations become essential, accurately modeling the entire assembly process and tracking the evolution of the structure as it grows. This not only helps predict how components will interact but also allows for optimization of the assembly sequence to avoid potential issues such as interference or instability. As space missions demand larger and more complex structures, robust simulation tools will be key to developing reliable ISA concepts, ensuring that structures are built efficiently and remain stable throughout their assembly and during operation in orbit.

In this work, a two-dimensional finite element model is introduced to predict the kinematics of large polygonal ring-like structures with a cable interior during the assembly process by a single stationary robot. This model is based on the ISA concept presented in Chapter 3 and is developed using commercial finite element software. The focus of this chapter is on the numerical model setup and the novel simulation techniques designed to capture the complexities of sequential assembly for large-scale structures.

The example structure used in this study consists of six bays, providing a practical scenario to refine the simulation technique and gain an accurate understanding of the evolving assembly process. This example aids in evaluating the structural behavior during each phase of the assembly, including the tensioning of the cables and the formation of the polygonal perimeter truss. Along with simulating the kinematics of the assembly, the study focuses on identifying and modeling critical design

considerations for the stationary robot. These considerations, aimed at optimizing the robot's performance to ensure a robust and efficient assembly process, are further explored in Chapter 5.

4.2 Numerical Simulation Setup

The proposed assembly concept involves sequentially constructing and releasing each truss bay, leading to intermediate configurations that are challenging to predict analytically. As each truss bay is pushed out perpendicular to the truss support axis, it rotates upon release due to elastic reactions in the joints, as shown in the third column of Fig. 3.5. This rotation causes vibrations with each released bay, potentially impacting the structural stability during the assembly process. Additionally, the simulation must handle tensioned cables throughout the process. These cables, critical for preserving the truss's structural integrity and final shape, exert forces that may induce oscillations and interfere with the assembly as they are secured to the truss joints. Disruptions can also arise from the locking of truss joints during assembly. This can lead to misalignments or increased stress in the structure, which may compromise the overall functionality.

In addition, achieving the desired final configuration of the structure is of utmost importance, as any deviations could affect the precision and functionality of the reflector. Lastly, adequate prestressing of the structure at the conclusion of the assembly process is critical, as it ensures that the truss remains rigid and stable under operational conditions. Without sufficient prestress, the structure may experience deformation or instability, undermining its performance.

Accurately predicting these dynamic responses is crucial to ensuring the overall reliability and precision of the assembly process, particularly in space, where even small deviations can compromise the structure's operational performance.

Given the prismatic geometry of the structure (see Fig. 2.1), the assembly process can be effectively modeled in two dimensions, as shown in Fig. 4.1. This two-dimensional model focuses solely on the truss elements forming a single perimeter ring of the polygonal truss in the horizontal plane (i.e., longerons) and is supported at one bay, incorporating a single integrated cable net. The forces exerted by the reflective metallic mesh on the cable net are not included in the model.

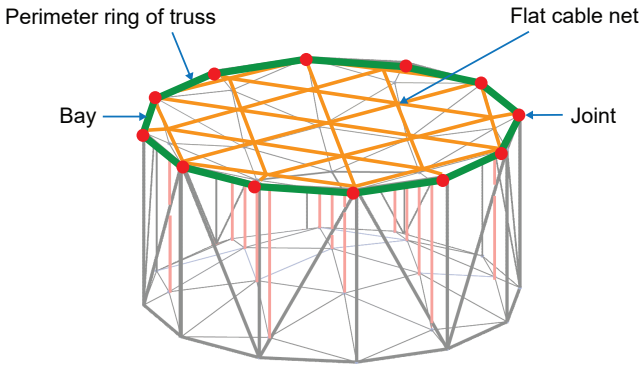

Figure 4.1: Simulation approach: perimeter ring and a single cable net.

4.2.1 Model Definition

This simulation aims to investigate the kinematics of polygonal ring-like structures with a cable interior, during assembly. Starting from the initial configuration of the truss supports which represent the truss builder, the assembly process sequentially adds each bay to the structure. As each bay is incorporated, cables are systematically attached to the corresponding truss nodes and tensioned, ensuring the structure maintains its geometric configuration and contributing to the truss' overall stiffness. The truss supports ensure precise positioning and securing of each bay, allowing the assembly to progress smoothly and ensuring that the final structure meets its intended shape and functionality.

A geometrically nonlinear finite element analysis was performed using ABAQUS/CAE 2020. The finite element model was established by modeling each perimeter truss bay as a two-dimensional rod, with a length matching the longeron of the lab-scale prototype (L_B = 0.3264 m) described in Chapter 6, and discretized into 10 two-node beam elements (B33). The joints between adjacent bays were modeled as pinned connections with Multi-Point Constraints (MPCs), allowing relative rotational DoF. Torsional stiffness at the joints was provided by defining ROTATION connector elements (see Fig. 4.2(b)), with the stiffness value set at k = 0.018 Nm/rad. Angular velocity-proportional damping (c = 50 Nms/rad) was applied at the joints, and joint masses were modeled as equivalent point masses at the corresponding truss nodes (N_i). The cross-sectional dimensions were selected to ensure that the stiffness of each bay was preserved. The following material properties for the bays were defined: high-modulus CFRP with E_{CFRP} = 325.4 GPa, Poisson's ratio ν = 0.3, and density ρ_{CFRP} = 1786 kg/m^3, similar to the structural design outlined in Section 2.3. Since all perimeter truss joints have identical rotational

stiffness, and the two end joints at the truss builder (N_1 and N_{12}) are disconnected in the final configuration (see Fig. 4.2(a)), short rods (b_1, b_2) of 10% the bay length, with the same material, cross-section, and mesh characteristics, were modeled at the ends. These short rods enable the definition of rotational springs at the joints between b_1-B_1 and b_2-B_{11}, but do not influence the kinematics of the structure during assembly.

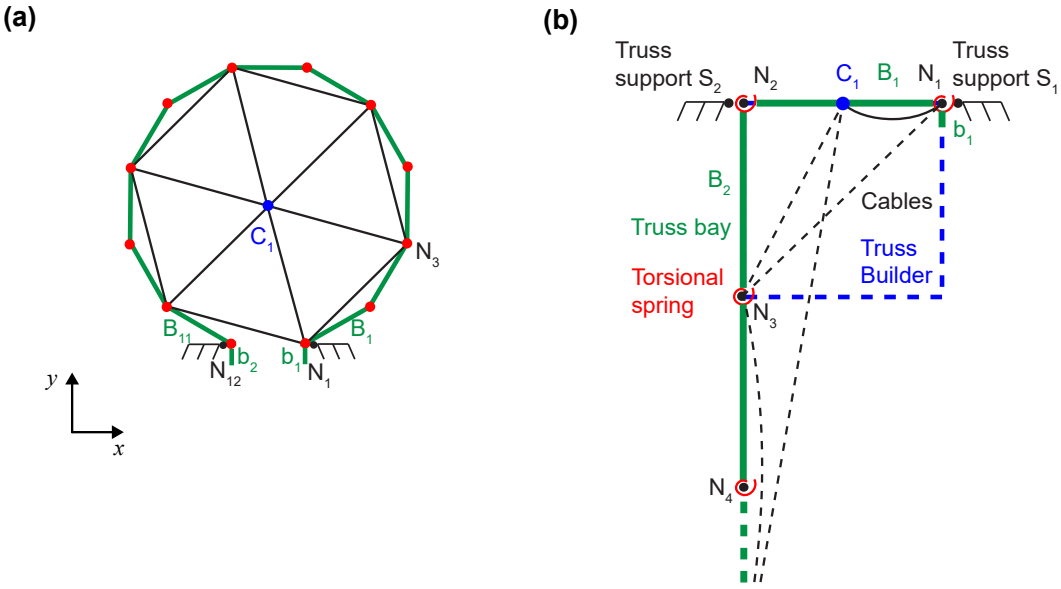

Figure 4.2: Finite element model definition for a) an example polygonal ring geometry, and b) corresponding initial configuration where rods and cables are modeled with their final connectivity.

4.2.2 Modeling the Cable Net

The two-dimensional cable net obtained by flattening the three-dimensional cable net does not not yield a unique equilibrium solution, which is essential for the design. To ensure that the structure is adequately prestressed and achieves its functional configuration, all truss members must be in compression, and all cable net elements must be in tension.

The cable net configuration was simplified as follows: consider a linear combination of the N_e equilibrium solutions $[F_c]_j$ that exist for a simplified two-dimensional cable net configuration. The coefficients a_j are optimized to minimize the average cable force $F_{c,\,avg}$, using MATLAB's *fmincon* function, while ensuring that all N_c cable net elements remain in tension and exceed a specified minimum force $F_{c,\,min}$. If real and bounded coefficients a_j are found, the desired prestress state exists for this simplified cable net configuration, and it is used in the model.

The mathematical formulation of this linear program is:

$$\left[\sum_{j=1}^{N_e} a_j [F_c]_j\right]_i = F_{c,\,i} > F_{c,\,min} \text{ for all } i \tag{4.1a}$$

$$a_{lower} < a_j < a_{upper} \tag{4.1b}$$

$$F_{c,\,avg} = \frac{\left(\sum_{i=1}^{N_c} F_{c,\,i}\right)}{N_c}. \tag{4.1c}$$

For this study, the linear programming coefficients a_j were assigned lower and upper bounds of [-500, 500] to ensure sufficient flexibility, and $F_{c,\,min}$ was set to 0.01 N. Figure 4.3(a) shows the adopted cable net configuration for the six-sided structure, featuring a prestress state in which all cables are under tension as desired, and all bays are under compression. In evaluating the self-stress states of the twelve-sided structure, the cable net simplification in Fig.4.3(b) led to slack cables, while the simplification in Fig.4.3(c) achieved the desired prestress distribution.

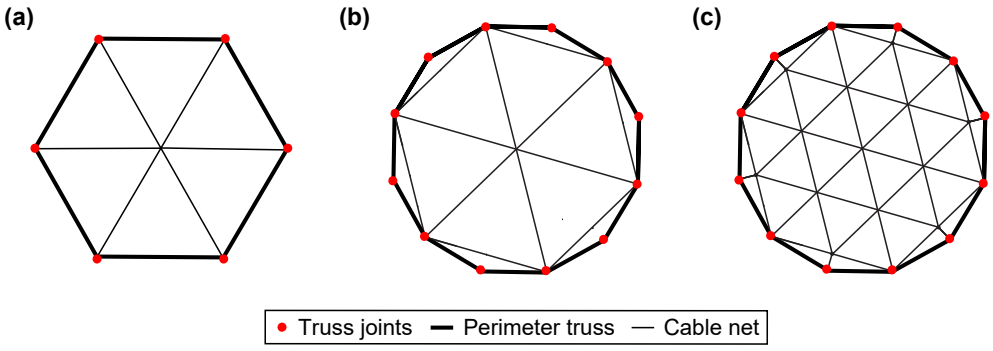

Figure 4.3: Simplification of cable net: (a) six-sided structure, and twelve-sided structure: (b) simplification-1, and (c) simplification-2.

Each cable is modeled using an AXIAL connector element with a specified nonlinear penalty function for stiffness, represented by the blue solid line in Fig. 4.4 and described by:

$$F_c = \frac{F_{c,\,max}}{1 + e^{-[c(u-u_0)]}}; c = 8000, u_0 = 0.5u_{lim}, F_{c,\,max} = 2000 \text{ N}. \tag{4.2}$$

This behavior reflects the properties of a high-modulus CFRP cable element (E_{CFRP} = 325.4 GPa) with a cross-sectional area of 6 mm x 150 μm, as specified in Section 2.3.1, under maximum tensile load, $F_{c,\,max}$. The unstressed reference length $l_{ref,\,ij}$ for each cable element ij is set to match the final flat configuration, i.e., at

the end of assembly, $u \approx 0$ and the cables experience minimal forces. In ABAQUS, the material stiffness is defined to maintain constant y-values beyond user-specified x-value limits. Hence the cable axial force, F_c, is defined to increase smoothly to $F_{c,\,max}$ at the limiting extension u_{lim}, approaching a strain of approximately 0.7%. The extension u_0 defines the midpoint of F_c's transition from zero to $F_{c,\,max}$.

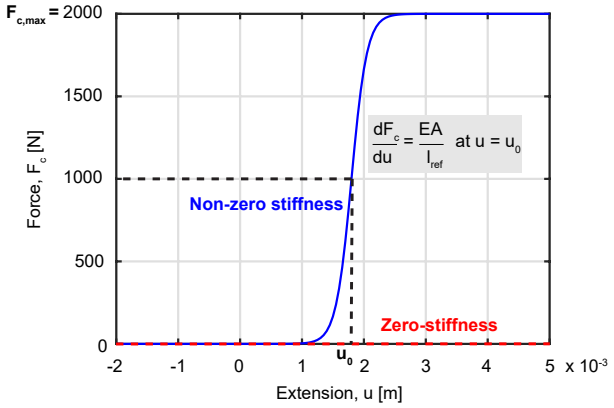

Figure 4.4: Specified nonlinear penalty function for cable stiffness in the finite element model.

The implicit direct-integration method used in ABAQUS/Standard is the Hilber-Hughes-Taylor (HHT) operator, an extension of the trapezoidal rule that solves dynamic equilibrium equations iteratively via Newton's method. Artificial damping is controlled by a numerical parameter, α, which influences the damping effect depending on the time increment and mode's oscillation period. The analysis described here focuses on two-dimensional motion using this Dynamic, Implicit integrator with maximum damping ($\alpha = -0.33$), providing up to 6% damping when the time increment is 40% of the oscillation period of the mode. Additionally, in the simulation, point masses are assigned at the intersecting nodes C_j, applying mass-proportional damping to account for material damping effects throughout the model.

It is important to note that the damping parameters in this simulation are selected primarily to ensure that the simulation steps can progress smoothly, rather than to achieve a specific damping ratio for the structure. The choice of damping is more focused on facilitating numerical stability and convergence during the analysis, rather than accurately reflecting physical damping characteristics of the actual system.

4.2.3 Simulation Steps

ABAQUS does not permit adding constraints or connector elements after the initial model setup, posing a challenge for simulating the sequential addition of

truss bays and the attachment of cable net nodes to truss joints, both essential for modeling the step-by-step assembly process. To overcome this, a simulation approach was developed where all truss bays were initially modeled as a series of connected rods with springs. Displacement and rotation boundary conditions were applied to simulate the 'push-out' and 'release' of each bay. A similar approach was utilized for attaching the cable net nodes. Initially, all cables were modeled with zero stiffness (represented by the red dashed line in Fig. 4.4) to prevent large fictitious extensions from imposing excessive forces on the structure. This initial modeling accounted for the significant extensions that occur when the cables are connected to the truss joints at the start of assembly, instead of connecting them just before pushing out the corresponding bay. These cables, shown by black dashed lines in Fig.4.2(b), are required to stretch by larger amounts. As the truss joints connected to the cables are pushed out, the cable stiffness is modified to its intended value (represented by the blue solid line in Fig. 4.4), effectively *activating* the cable and allowing it to become a part of and exert forces on the structure. Active cables are indicated by black solid lines in Fig. 4.2(b). Note that this approach fundamentally differs from the physical process, as it simulates a change in cable stiffness rather than the physical attachment of slack cables (see Appendix B for details).

The simulation sequence involved repeating bay translation, activating or modifying cable stiffness, and releasing the translated bay to simulate the 'bay push-out,' 'cable attachment,' and 'intermediate polygonal truss formation,' as shown in Fig. 4.5. The bays were pushed out at a speed of 10 mm/s.

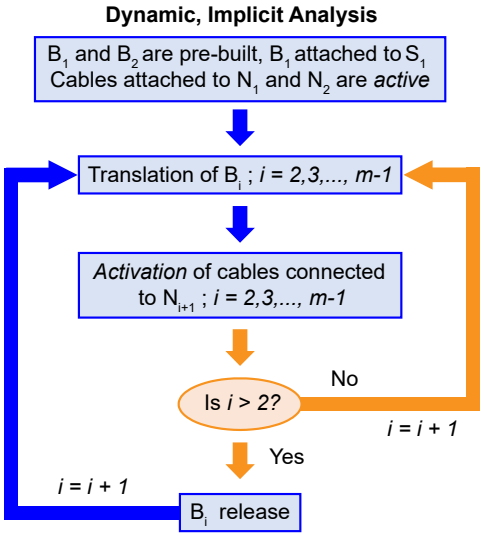

Figure 4.5: Framework of simulation steps.

The initial configuration of the bays and cables for the polygonal ring geometry shown in Fig. 4.2(a) is depicted in Fig. 4.2(b). Points S_1 and S_2 simulate the fixed supports of the truss builder in two-dimensional space. Figure 4.6 shows the boundary conditions used to simulate the assembly process. Truss node N_1 and bay element b_1 are fixed in translation at S_1 ($U_1 = U_2 = 0$ in Fig. 4.6(a)), while bay B_1 is free to rotate throughout the simulation ($UR_3 \neq 0$ for N_1). As bay B_2 is pushed out via the translational DoF (U_1, U_2) of node N_3, node N_2 is allowed to rotate in-plane, forming the first intermediate polygon, a triangle (see Figs. 4.6(a) and (b)). Once B_2 is pushed out, node N_3 is fixed in translation at S_2 while the cables connected to N_3 are activated. The modified DoFs during this activation step have been highlighted in red in Fig. 4.6(b).

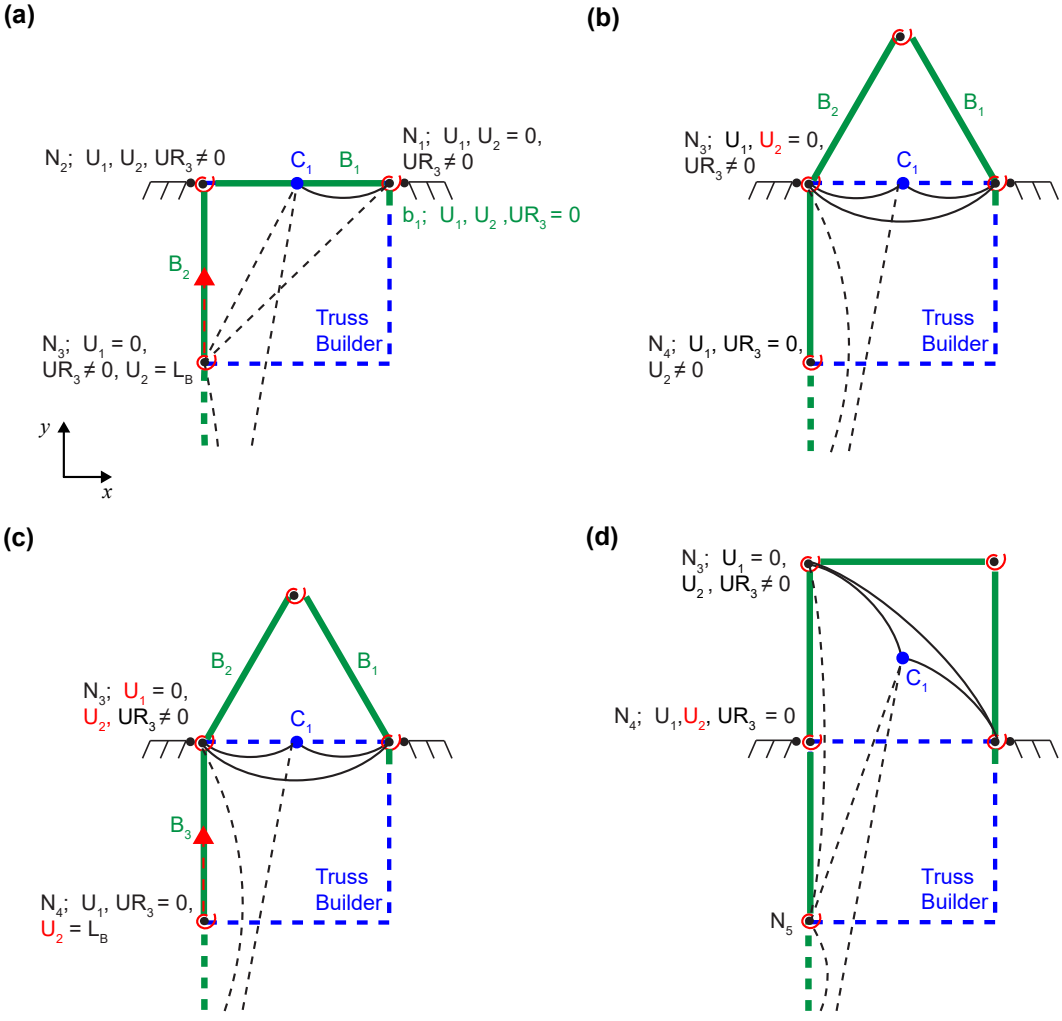

Figure 4.6: Boundary conditions when a) pushing-out bays B_1 and B_2, b) activating cables connected to N_3, c) pushing out bay B_3, and d) activating cables connected to N_4.

For subsequent bays ($i > 2$), the process repeats: bay B_i is pushed out while constrained to the assembly plate (not modeled) by controlling the translational DoFs of nodes N_i and N_{i+1} (highlighted in red in Fig. 4.6(c)). As the corresponding cables are activated, node N_{i+1} is fixed in translation at S_2, while node N_i is also fixed (see U_1 and U_2 in Fig. 4.6(d)). The translational DoF in 1-direction, U_1 at node N_i is released to simulate the retraction of the assembly plate, forming an intermediate polygon with i sides (Fig. 3.5, third column). Throughout, bay element b_2 moves with B_{11}, and at end of the assembly, node N_{12} remains fixed at S_2 alongside b_2. The free nodes of cable net C_j are initially placed at even spacing between S_1 and S_2, and they are free to rotate and translate in the plane as the cables are 'attached' to the perimeter truss during assembly.

4.3 Tuning the Simulation for a Six-Sided Structure

The assembly process simulation involves the interaction of multiple parameters. To ensure accurate results, it was necessary to fine-tune the parameters of the simulation technique. The tuning process used a six-sided structure with six cables and a single interior cable node C_1 (see Fig. 4.7). We begin by identifying the associated parameters.

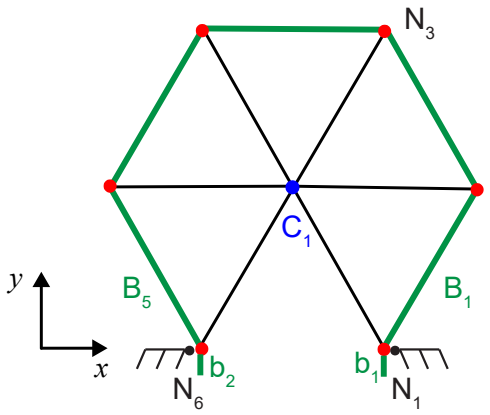

Figure 4.7: Geometry of six-sided structure.

4.3.1 Angle Stops

Figure 4.8(a) shows a section of a typical ring-like truss, with the perimeter truss shown in green and the cables in black. The cable connecting nodes N_{i-1} and N_{i+1} is designed to be shorter than the sum of the lengths of bays B_{i-1} and B_i, as dictated by the cable net configuration:

$$\overline{N_{i+1}N_i} + \overline{N_iN_{i-1}} > \overline{C_{edge,\,i+1}C_j} + \overline{C_jC_{edge,\,i-1}}. \tag{4.3}$$

In the proposed assembly scheme, before bay B_i is pushed out, the edge cable node $C_{edge,\,i+1}$ is held at the front of the truss builder (see Fig. 4.8(b)). As the truss builder pushes out bay B_i mounted on the assembly plate, the cable between nodes $C_{edge,\,i+1}$ and $C_{edge,\,i-1}$ transitions from slack to tensioned. If node N_i is pushed outward relative to the assembly plate, this tensioned cable could potentially jam the plate or become damaged. Hence, to ensure a smooth assembly, the intermediate perimeter truss configurations are required to be convex polygons (see Fig. 3.5, second column), by introducing angle stops at each joint with a torsional spring. Since all bays are defined as a series of co-linear rods in the initial step of the simulation, the angle stop range, α, is limited to a maximum of π radians (see Fig. 4.8(c)), thereby preventing outward kinking of the truss nodes. However, no angle stops are applied at nodes N_1 and N_m $(m = 6)$, allowing them to bend outward as needed to achieve the intermediate polygonal shapes and final truss configuration (see Fig. 4.7). This angle stop definition was applied consistently throughout the simulation study.

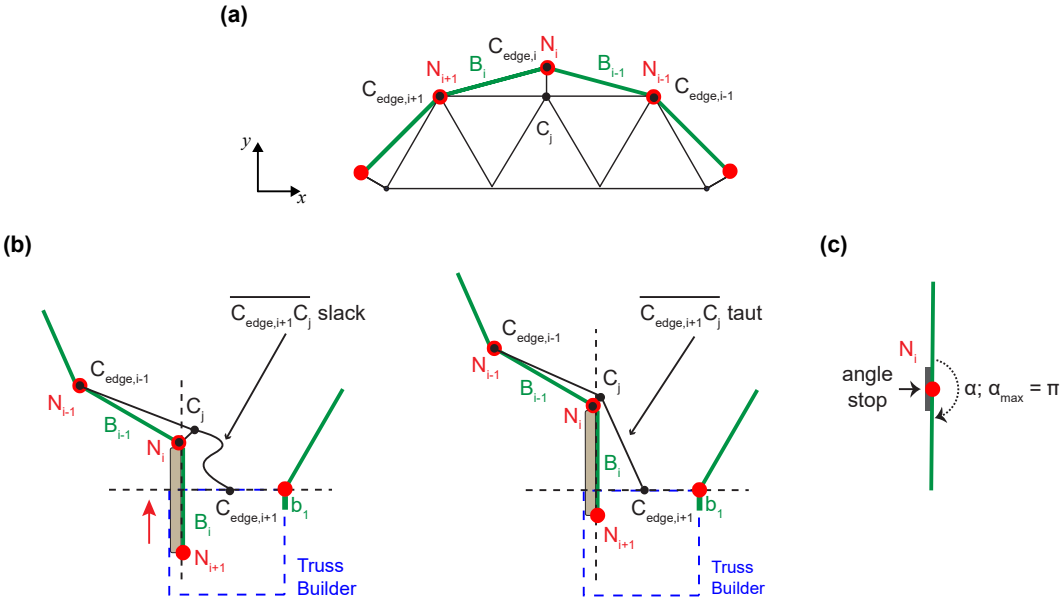

Figure 4.8: Angle stops: a) geometry of the structure, b) cables transitioning from slack to taut during bay push out, and c) definition of angle stop.

4.3.2 Assembly Plate Orientation

The orientation of the assembly plate, i.e., the angle θ at which each truss bay is pushed out with respect to the face of the truss builder is a crucial parameter in the

truss builder design. It imposes a constraint on the range of motion of the structure during assembly. As illustrated in Fig. 4.9(a), pushing out each assembled bay perpendicular to the truss face, as initially proposed, forces the structure to become heavily distorted. Tilting the assembly plate provides more space and allows a more uniform shape (see Fig. 4.9(b)). The angle of the assembly plate, θ, plays a significant role in the process: a distorted shape increases the tension in the cable net and requires additional corrections to align the ring to its intended configuration. Consequently, it is essential to evaluate how the assembly plate angle affects shape distortion to ensure efficient assembly. For the six-sided structure, three assembly plate orientations were selected: $\theta = 90°, 80°, 60°$.

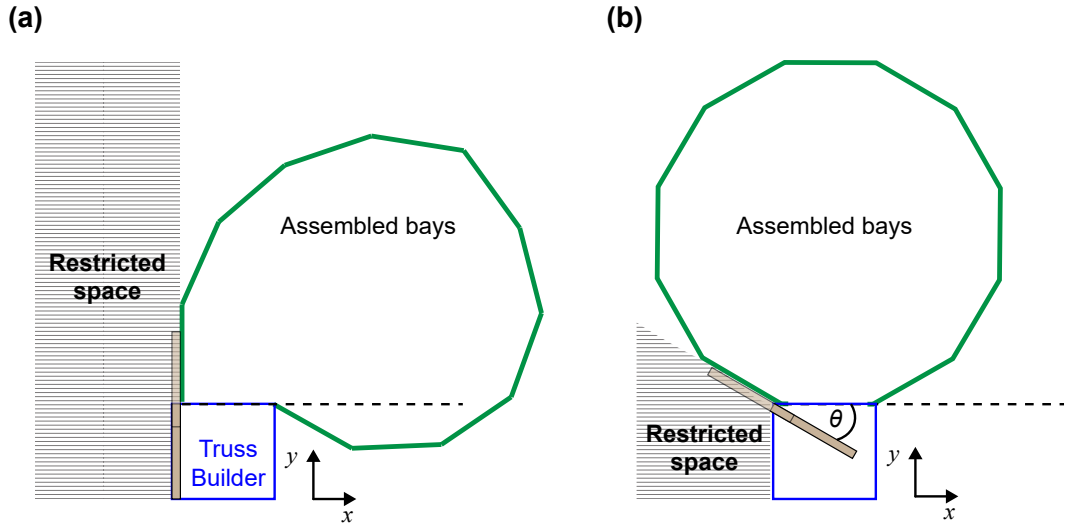

Figure 4.9: Two assembly plate orientations: a) perpendicular to the truss builder face: $\theta = 90°$, and b) tilted at angle $\theta < 90°$.

4.3.3 Damping Coefficients

Since the simulation involves a dynamic integration of the motion of the structure, mass-proportional damping was applied to the moving nodes, particularly C_j. For a given nodal mass, the Rayleigh damping coefficient α_R was selected to be sufficiently high to avoid numerical instabilities. To understand the effect of different damping coefficients, a sensitivity study was conducted for $\alpha_R = 0.5, 5.0, 7.5, 10$, with a nodal mass of 0.020 kg.

Table 4.1 summarizes this sensitivity study, highlighting the effects of different assembly plate orientations and damping factors. The maximum and root-sum-of-squares (RSS) variation of the final axial extensions u_i of the cables from their

expected final values (set at $u_{i,\ expected} = 0;\ i = 1, 2, \ldots, 6$ by design) was used as the metric for comparison. Only simulations that successfully achieved the desired final shape with an RSS error less than or equal to 12 mm were considered. The table shows that all assembly plate orientations produced the desired shape for certain damping factors. While the magnitudes of the variation in extensions change with θ, the smallest variations, approximately one-third lower compared to other angles, and thus the most favorable results, are observed for $\theta = 60°$. The effect of the damping factor magnitude on the variations for a given θ is minimal, as evidenced by the small changes in the corresponding extensions. Therefore, the lowest damping coefficients which allowed for successful completion of the simulations were adopted for each assembly plate orientation.

Table 4.1: Sensitivity to assembly plate orientation and damping coefficient

$\theta(°)$	$\alpha_R(\mathrm{s}^{-1})$	Final shape achieved	$\lvert\Delta u_i\rvert_{max}$(mm)	$\sqrt{\sum_{i=1}^{6} \Delta u_i{}^2}$(mm)
90	0.5	✓	6.84	7.48
	5.0	✓	6.84	7.48
	7.5	✓	6.84	7.48
	10.0	✓	6.84	7.48
80	0.5	×		
	5.0	✓	6.88	7.52
	7.5	✓	6.87	7.51
	10.0	✓	6.87	7.52
60	0.5	✓	4.60	5.09
	5.0	✓	4.56	5.06
	7.5	✓	4.49	5.00
	10.0	✓	4.59	5.09

4.4 Simulation Results for the Six-Sided Structure

Figure 4.10 presents the simulation results for the progression of cable extension during the assembly of the six-sided structure with $\theta = 90°$, alongside snapshots of the intermediate shapes of the structure. Cables are color-coded for clarity. Each snapshot shows only the active cables, while the graph distinguishes between active cables and inactive cables with solid and dotted lines, respectively. At the start of the assembly, B_1 and B_2 are pre-assembled, and cables 1 and 2 are active according to the ISA concept. Vertical lines on the graph mark transitions between different assembly phases: from 'bay translation' to 'cable activation' and then to 'bay release.' The greyed-out region in the graph indicates slack cables ($u_i < 0$).

The results show that all cables successfully reach their unstressed length by the the 100% assembly point, as required. The graph illustrates the evolution of cable net extensions, providing insight into the intermediate shapes of the structure during assembly and confirming whether the final configuration meets expectations. As expected, cables 3-6 experience positive extension at the start of assembly since they are modeled with their final connectivity. However, they are inactive, as indicated by dotted lines, and hence do not exert forces on the structure until activated. This is reflected in the snapshots of the intermediate shapes.

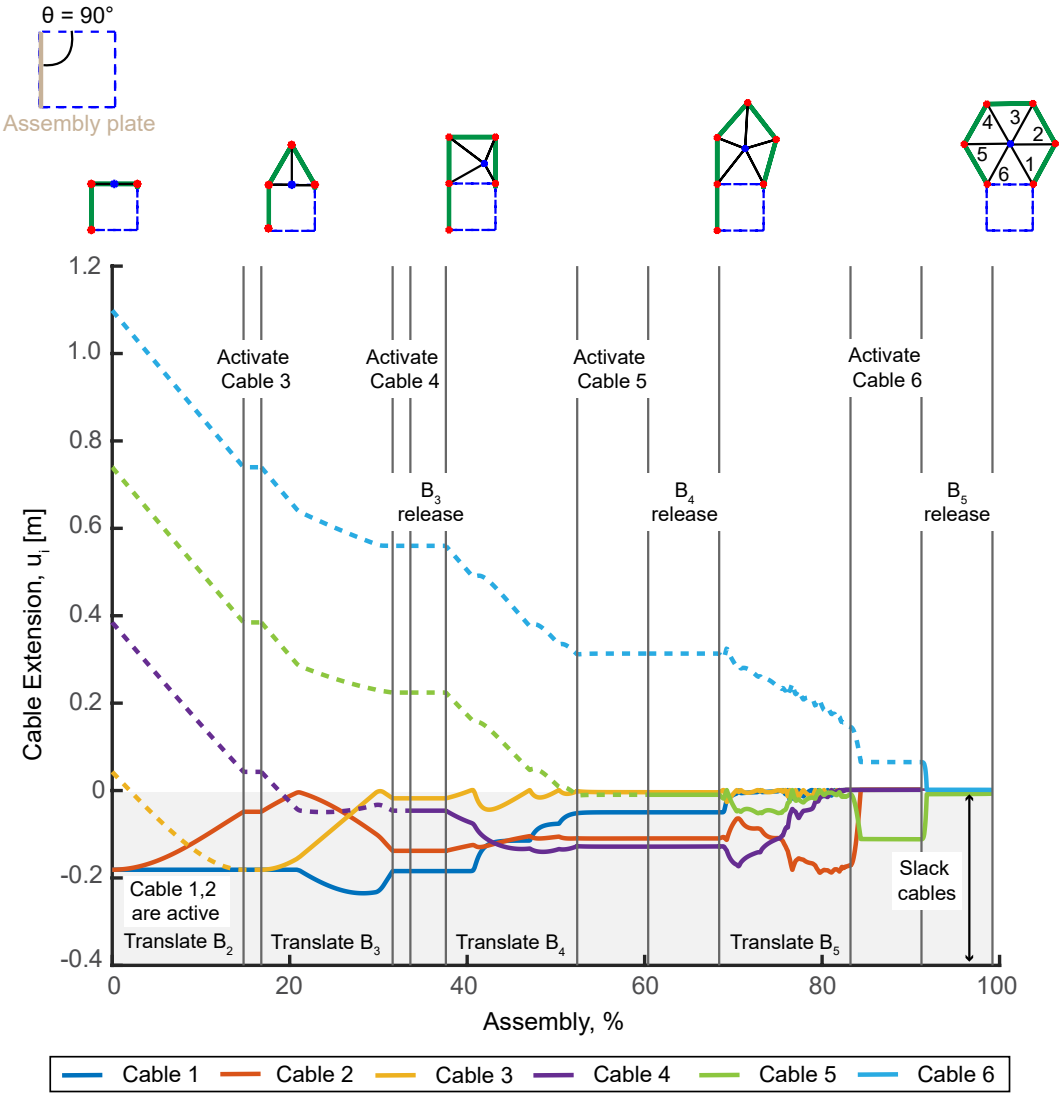

Figure 4.10: Cable extension results for the six-sided structure; $\theta = 90°$.

Another important detail is that each cable is activated when it is near or within the slack region, which in the simulation helps to minimize the dynamic forces

applied to the structure during the activation steps. Throughout the process, at least one active cable remains slack until the final cable is activated and the last bay is released, marking the desired end of the assembly.

Close observation of the intermediate shapes reveals that regular polygons are not achieved upon releasing the respective bays. This is due to the angle stops at the joints, which restrict the anti-clockwise rotation of the truss node at S_2 (see the next bay ready for assembly in the snapshots). The intermediate rings tend to rotate anti-clockwise at S_2, but the angle stops prevent them from going beyond the assembly plate angle. Taut cables may also be responsible for the non-regularity observed in the intermediate polygons. The final polygonal configuration is regular, as intended, with all cables active and nearly prestressed.

Figure 4.11 presents the simulation results for the assembly with $\theta = 60°$. Although the final configuration—a regular hexagon—is achieved also in this case, it is evident that the intermediate shapes vary depending on the value of θ, as emphasized in Fig. 4.12. This variation highlights the significance of the assembly plate orientation to the assembly process.

The effect of the more symmetric structure deployment on the cable interior is particularly evident from the comparison of cable extensions in Figs. 4.10 and 4.11 during the translation of B_5. For the $\theta = 60°$ case, the cable extensions exhibit a smoother transition and reach the desired prestress level more rapidly compared to the $\theta = 90°$ case. This results in a more controlled and gradual activation of the final set of cables, facilitating a more stable and precise completion of the assembly process.

This variability in intermediate shapes is expected to be more pronounced in larger polygonal rings, where the assembly plate angle significantly impacts the geometry and stability of the structure during assembly. The influence of the assembly plate angle on these intermediate shapes and its implications for the assembly of larger structures are discussed in Chapter 5.

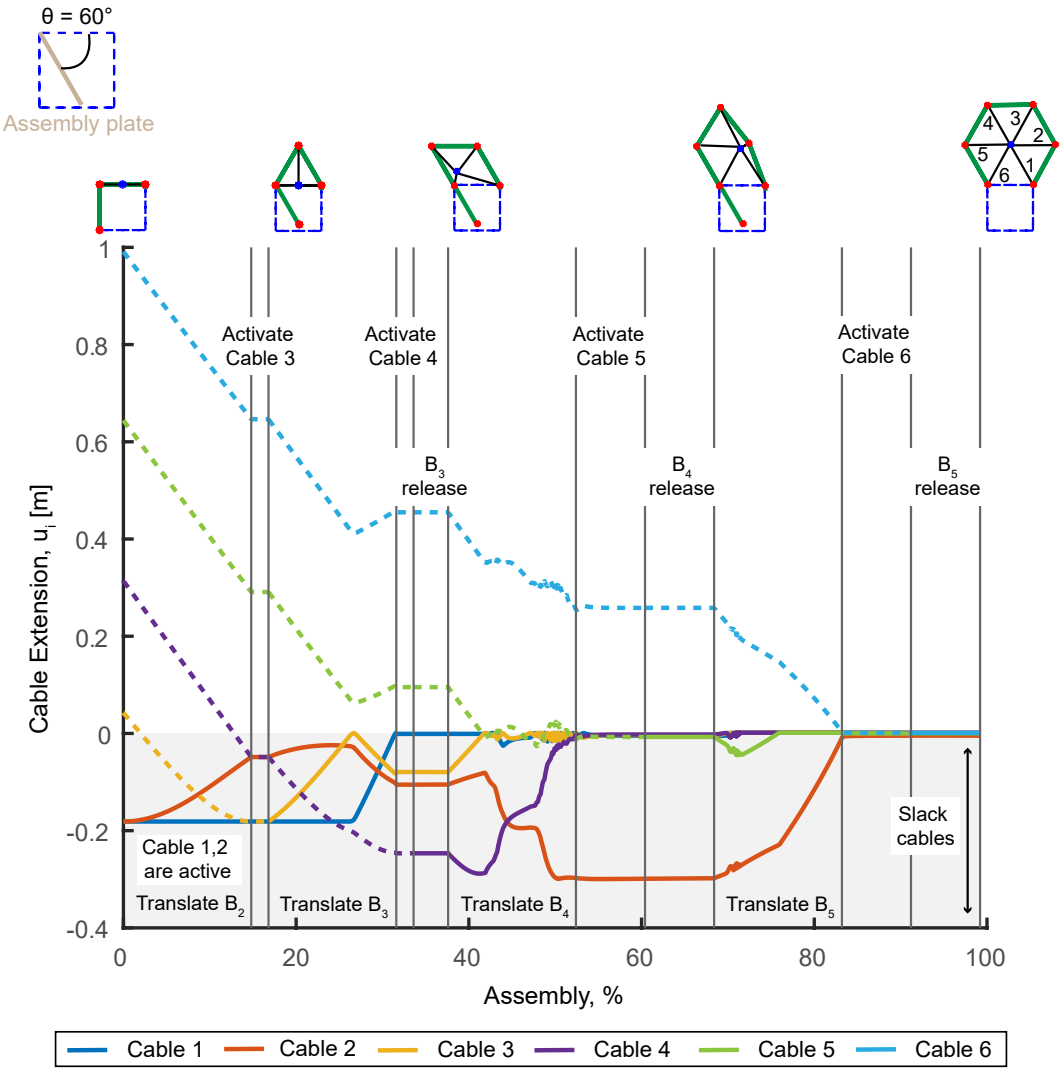

Figure 4.11: Cable extension results for the six-sided structure; $\theta = 60°$.

4.5 Chapter Conclusions

This chapter has introduced the numerical simulation setup for the proposed ISA concept for large polygonal ring-like structures using a two-dimensional finite element model. This model, implemented in ABAQUS/CAE 2020, simulates the kinematics of a six-sided structure with a cable net interior assembled by a single stationary robot. The focus was on modeling the sequential assembly of the truss bays and the attachment of the cable net and ensuring that accurate final configurations could be achieved.

The simulation revealed that achieving the final desired shape—specifically, a regular hexagon—was successful for various assembly plate orientations. However, the intermediate shapes differed significantly depending on the assembly plate orien-

tation, an effect that is expected to be more pronounced in larger polygonal rings. A sensitivity study of damping coefficients demonstrated that varying these values has minimal impact on the magnitude of cable extension variations for a given assembly plate orientation. The lowest damping coefficients that permitted successful simulation completion were adopted for the study. This approach ensured that the simulations accurately reflected the assembly process without numerical instability.

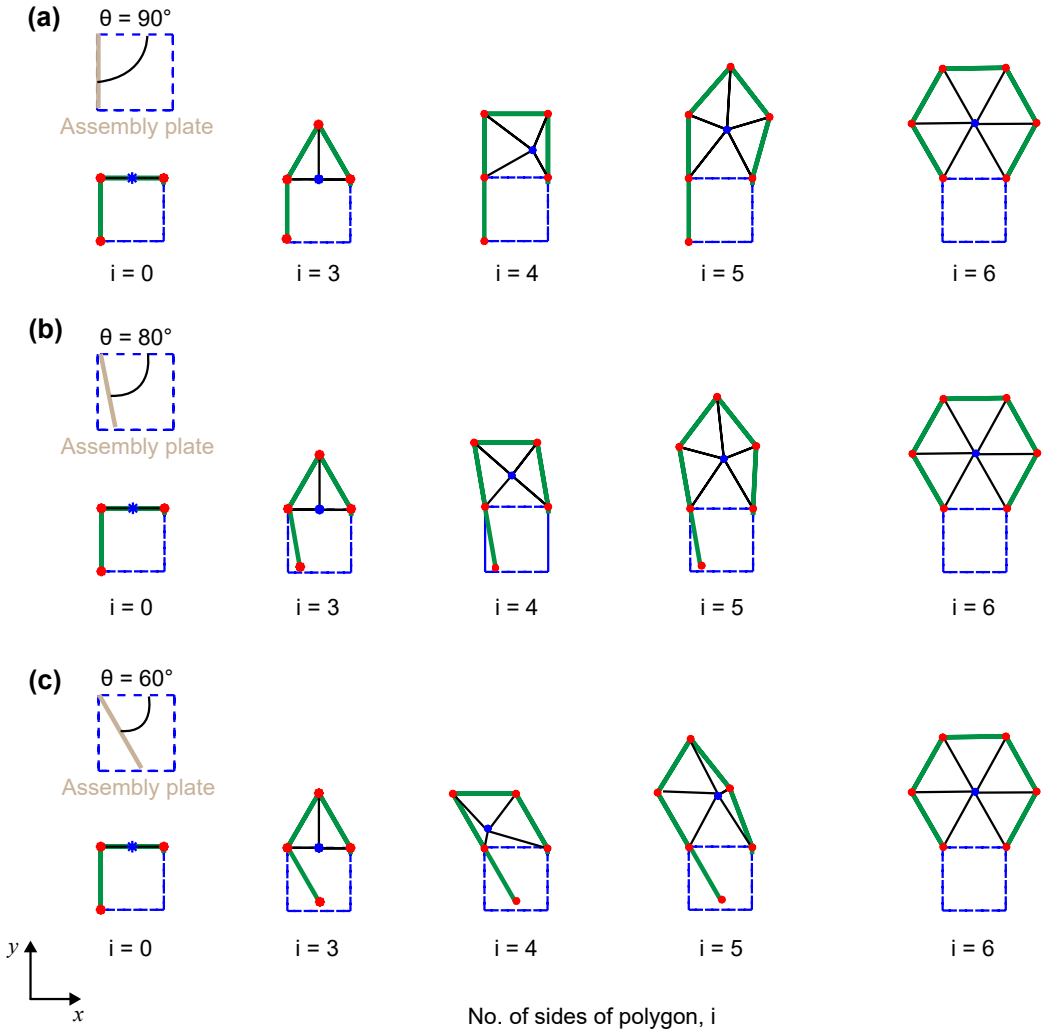

Figure 4.12: Intermediate polygonal shapes: (a) $\theta = 90°$, (b) $\theta = 80°$, and (c) $\theta = 60°$.

The innovative simulation techniques developed offer sufficient confidence at this stage to evaluate the feasibility of the proposed ISA concept for larger ring-like structures. Chapter 5 further explores this by identifying key design considerations and potential improvements to the stationary robot to enhance efficiency and robustness of assembly.